JACS
JOURNAL OF THE AMERICAN CHEMICAL SOCIETY

ARTICLE

pubs.acs.org/JACS

Mechanically Activated Molecular Switch through Single-Molecule Pulling

Ignacio Franco,*[,†] Christopher B. George,[†] Gemma C. Solomon,[‡] George C. Schatz,[†] and Mark A. Ratner*[,†]

[†]Department of Chemistry, Northwestern University, Evanston, Illinois 60208-3113, United States

[‡]Nano Science Center and Department of Chemistry, University of Copenhagen, Universitetparken 5, 2100 Copenhagen, Denmark

Supporting Information

ABSTRACT: We investigate a prototypical single-molecule switch marrying force spectroscopy and molecular electronics far from the thermodynamic limit. We use molecular dynamics to simulate a conducting atomic force microscope mechanically manipulating a molecule bound to a surface between a folded state and an unfolded state while monitoring the conductance. Both the complexity and the unique phenomenology of single-molecule experiments are evident in this system. As the molecule unfolds/refolds, the average conductance reversibly changes over 3 orders of magnitude; however, throughout the simulation the transmission fluctuates considerably, illustrating the need for statistical sampling in these systems. We predict that emergent single-molecule signatures will still be evident with conductance blinking, correlated with force blinking, being observable in a region of dynamic bistability. Finally, we illustrate some of the structure−function relationships in this system, mapping the dominant interactions in the molecule for mediating charge transport throughout the pulling simulation.

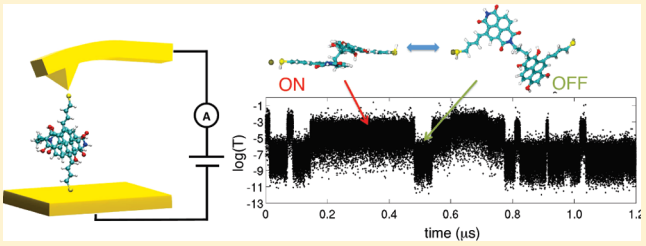

INTRODUCTION

The emerging ability to study physical properties at the single molecule level highlights the disparity between what is observable in an ensemble of molecules and the contributions of constituent parts.[1] A key feature of single-molecule experiments is that fluctuations in observables are comparable with their average values, in contrast with macroscopic behavior where fluctuations are usually negligible. This can lead to fluctuation-induced emergent phenomena, thereby providing a signature of single-molecular characteristics.

The integration of single-molecule pulling techniques[2−6] with molecular electronics[7−13] offers unique opportunities both for the development of novel mechanically controlled electronic devices and for the use of the remarkable sensitivity of the molecular transport properties to molecular conformation to characterize the state of molecules as they are mechanically elongated. In this paper we present an integrated analysis of force−extension and molecular junction transport behavior as a molecule bound to a counter electrode is pulled by an atomic force microscope (AFM) tip.

The general setup of this class of experiments is schematically illustrated in Figure 1A. One end of the molecule is chemically bonded to a metallic surface, while the other end is bonded to a conducting AFM (CAFM) tip attached to a cantilever. A voltage is applied across the junction and the resulting current measured. In such a setup, the distance between the surface and the cantilever L is controlled while the force F exerted fluctuates. For a given L, the force is quantified by measuring the deflection of the cantilever from its equilibrium position, $F(t) = -k[\xi(t) - L]$, where $\xi(t)$ is the fluctuating molecular end-to-end distance coordinate and k is the cantilever stiffness. Control over L permits the manipulation of the molecular conformation and hence control of the overall transport properties of the junction.

To date, only a few examples that explore this integration have been reported. Experimentally, Lafferentz et al. have measured the conductance of a single conjugated polymer adsorbed on a metal surface as it is retracted using an AFM tip.[14] Chang et al.[15] have explored the possibility of using tunneling currents as a function of elongation as an analytical probe for DNA base pairs. Quek et al.[16] have constructed a reversible switching device based on mechanically changing the contact geometry of a 4,4′-bipyridine−gold junction, and Parks et al.[17] have demonstrated mechanical control of molecular magnetic anisotropy via modification of molecular symmetry. In turn, computations by Lin et al.[18] have shown how molecular elongation induces tunneling current decay in an alkanedithiol.

There is, however, a lot more richness to single-molecule pulling than simple molecular elongation. These experiments[2,3,19,20] show considerable thermal fluctuations in the force measurements due to the nanoscopic nature of the molecule that is elongated.[6] Further, the resulting force−extension isotherms often exhibit stress maxima that have been linked to molecular unfolding events, as well as blinking[3,21,22] in the force measurements, from a high force to a low force regime, for selected extensions.

Received: October 22, 2010
Published: February 1, 2011

dx.doi.org/10.1021/ja1095396 | J. Am. Chem. Soc. 2011, 133, 2242–2249

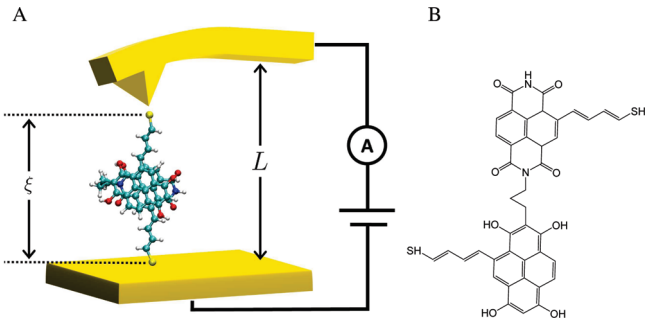

Figure 1. Setup and proposed conducting medium for the mechanically controlled nanoscopic switch. (A) Schematic of a single-molecule pulling/molecular electronics setup. In it, a molecule is attached to a metallic surface and a conducting AFM tip. The distance between the surface and the cantilever L is controlled, a voltage is applied across the junction, and the resulting current is measured. Varying L permits control of the conductance of the junction via induced changes in the molecular conformation. The instantaneous applied force is given by $F(t) = -k[\xi(t) - L]$, where k is the cantilever force constant and $\xi(t)$ is the fluctuating molecular end-to-end distance. (B) The molecular superstacker proposed as a conducting medium. The stacker consists of 1,4,5,8-naphthalenetetracarboxylic diimide joined to 1,3,6,8-pyrenetetrol via a short aliphatic chain. Hydrogen bonds between the hydroxy and carbonyl groups in each aromatic unit stabilize the stacked conformation. The attached alkenethiols link the stacker to the surface and the CAFM tip as specified in (A).

Here we demonstrate how the basic phenomenology of single-molecule pulling can be exploited to create a novel mechanically activated molecular switch, and we illustrate how the thermal fluctuations, stress maxima, and dynamical bistability observed in the force measurements manifest in terms of molecular transport properties. As a conducting medium we propose the molecular superstacker shown in Figure 1B. The stacker is composed of two complementary aromatic rings—a naphthalene diimide and a pyrene tetrol—that π-stack strongly due to the four hydrogen bonds that can form between the hydroxy (−OH) and carbonyl (−C═O) groups in the complementary aromatic units. The stacker is bonded to the Au surface and CAFM tip through thiol-terminated alkene conjugated chains in the manner suggested in Figure 1A.

The simulations are performed by combining constant temperature molecular dynamics (MD) simulations of the pulling with computations of the transport properties based on a Green's function formalism.[7] To bridge the several orders of magnitude gap between experimentally employed pulling speeds (10^{-6}–10^{-9} m s^{-1}) and those that can be accessed computationally, the pulling is performed under reversible conditions so that the results become independent of the pulling speed. Electron transport is assumed to occur in the coherent tunneling regime, in which the bias-dependent current $I(V)$ can be calculated from the Landauer formula,[7]

$$I(V) = \frac{2e}{h}\int_{-\infty}^{\infty} \mathrm{d}E[f_{\mathrm{L}}(E,V) - f_{\mathrm{R}}(E,V)]T(E,V) \qquad (1)$$

Here e is the electron charge, h is Planck's constant, $f_{\mathrm{L,R}}$ are the Fermi functions of the left and right electrodes, respectively, and T is the transmission function; the Fermi function and the transmission are dependent on the injection energy E and the applied bias voltage V. We assume low biases for which $I \approx GV$, where $G = G_0T(E_{\mathrm{F}})$ is the zero-bias conductance, $G_0 = 2e^2/h$ is the quantum of conductance, and $T(E_{\mathrm{F}})$ is the transmission at the electrodes' common Fermi energy. The quantity $T(E_{\mathrm{F}})$ is calculated for conformations encountered during the MD simulation using two different computational methods, gDFTB[23−27] and Huckel-IV 2.0.[28] These tight-binding methods differ in the way they describe the electronic structure of the junction. The latter uses an extended-Huckel model Hamiltonian, but for simplicity we will refer to it as Huckel. The details of the computational setup are specified below.

METHODS

Pulling Simulations. Molecular dynamics simulations modeling several microseconds of pulling were performed using TINKER 4.2,[29] for which a pulling routine was developed, and the MM3 force field.[30−32] The MM3 force field adequately describes π-stacking interactions and includes directional hydrogen-bonding terms important in the description of the superstacker. Additional required force field parameters are included in the Supporting Information. During pulling, one terminal S atom of the molecule was attached to a stiff isotropic harmonic potential that mimicked the molecular attachment to the surface. Simultaneously, the opposite terminal S was connected to a dummy atom via a virtual harmonic spring. The varying deflection of the virtual harmonic spring measured the force exerted during the pulling. The pulling was performed by varying the distance between the surface and the cantilever L from 18 to 28 Å using a cantilever force constant of k = 1.1 N/m. The pulling direction was defined by the vector connecting the two terminal S atoms of the complex. The pulling speeds required to recover reversible behavior were $\nu = 2 \times 10^{-5}$ Å/ps for L = 18−22 and 24−28 Å, and $\nu = 1 \times 10^{-6}$ Å/ps for L = 22−24 Å. The dynamics of the system was propagated using a modified Beeman algorithm with a 1 fs integration time step. The system was coupled to a heat bath at 300 K using a Nosé−Hoover chain as the thermostat.

Transport Calculations. Transport calculations were performed using two tight-binding methods: gDFTB[23−27] and Huckel-IV 2.0.[28] gDFTB parameters are based on density functional theory, while Huckel-IV uses an extended-Huckel method. Electrodes were modeled by Au[111] surfaces included on both sides of the molecule with sulfur atoms chemisorbed to fcc hollow sites. Gold−sulfur distances were held constant for all calculations and were chosen according to the literature.[33] In Huckel-IV 2.0 calculations, each Au[111] surface was represented by three gold atoms, and the molecule−electrode coupling terms only included contributions from Au−S coupling. In gDFTB calculations, gold electrodes were described by three 9 × 9 Au(111) layers, and periodic boundary conditions were used. In gDFTB, the standard Fermi energy of −5.0 eV was used. In Huckel-IV, the offset between the Fermi level and the energy of the highest occupied molecular orbital (HOMO) is an adjustable parameter. We choose this parameter such that the Fermi level falls within the molecular energy gap. Specifically, the Fermi energy was taken to be the Huckel value of −9.5 eV,[28] and the molecular orbital energies were shifted by 1.35 eV. A discussion of the band-lineup problem is available elsewhere.[34−36]

Local Currents. In our analysis of the electronic transport through the superstacker, we decompose the total transmission into local transmission[27,37,38] elements to elucidate the relative contributions of chemically important units in the molecule. The local transmission elements are defined between pairs of atoms (A and B) such that the sum of local transmission elements across a surface equals the total transmission:[38]

$$T(E,V) = \sum_{\mathrm{A}\in\mathrm{L},\,\mathrm{B}\in\mathrm{R}} T_{\mathrm{AB}}(E,V) \qquad (2)$$

where A and B are atoms located to the left (L) or right (R) of the surface in question. In this article we use these local transmission elements for both qualitative and quantitative analysis of the transmission results.

dx.doi.org/10.1021/ja1095396 |J. Am. Chem. Soc. 2011, 133, 2242–2249

The local transmission elements $T_{AB}(E,V)$ can be plotted for the whole molecule to give a quantitative picture of the local transmission or summed over some subset of atoms to give a qualitative sense of the relative contributions of different parts of the structure to the total transmission.

Potential of Mean Force and $p_L(\log T)$. The molecular potential of mean force $\phi(\xi)$ along the end-to-end distance coordinate was reconstructed from the force measurements using the weighted histogram analysis method (WHAM),[39,40] as described in detail elsewhere.[22] The probability density distribution $p_L(\log T)$ in the $\log T$ measurements at a given extension L is defined by

$$p_L(\log T) = \frac{1}{Z(L)}\int dr\, \delta[\log T(r) - \log T] \exp\{-\beta[U_0(r) + V_L(\xi)]\}$$
$$= \frac{Z_0}{Z(L)}\int d\xi \exp\{-\beta V_L(\xi)\} p_0(\log T, \xi) \quad (3)$$

where r is the position vector of the N atoms in the system, $U_0(r)$ the potential of the molecule, $Z_0 = \int dr \exp\{-\beta U_0(r)\}$ the configurational partition function of the molecule, and $Z(L) = \int dr \exp\{-\beta[U_0(r) + V_L(\xi)]\}$ the configurational partition function of the molecule plus cantilever. Here, $V_L(\xi) = k(\xi - L)^2/2$ is the potential due to the cantilever of stiffness k at extension L. The quantity $p_L(\log T)$ is estimated by first computing the unbiased probability distribution,

$$p_0(\log T, \xi)$$
$$= \int dr\, \delta[\log T(r) - \log T]\delta[\xi(r) - \xi] \exp\{-\beta U_0(r)\}/Z_0 \quad (4)$$

from the combined force−transmission data using WHAM and then using this quantity to estimate $p_L(\log T)$ through eq 3.

RESULTS AND DISCUSSION

Molecular Conductance during Pulling. The force exerted on the junction and the transmission through the junction as the system is elongated under reversible conditions at 300 K are shown in Figure 2. Typical structures encountered during the pulling are included in the upper panel. During the extension the molecule undergoes a conformational transition from its stacked conformation to an open structure. In the process, the force initially increases to 186 pN, then exhibits a 44 pN drop due to molecular unfolding, and then increases again. The drop in the force is well within the resolution of AFM pulling experiments.[3]

These induced changes in molecular conformation provide the basis for a mechanically activated molecular switch. Specifically, during the pulling the transmission goes from a high-transmission "on" state when the molecule is stacked to a low-transmission "off" state when the molecule unfolds. During the unstacking the observed average transmission drops by 3−4 orders of magnitude. These two "on" and "off" molecular phases can be accessed reversibly by varying the distance between the surface and the cantilever L.

Both the force and the transmission measurements observe large-scale thermal fluctuations. These fluctuations are comparable to the average values, indicating that the system is far from the thermodynamic limit. The fluctuations in the force reflect conformational changes along the ξ coordinate. They are larger around the region of mechanical instability, where the average force decreases with increasing L, and can be reduced by employing softer cantilevers.[22] In turn, the transport properties of the junction are extremely sensitive to molecular conformation,

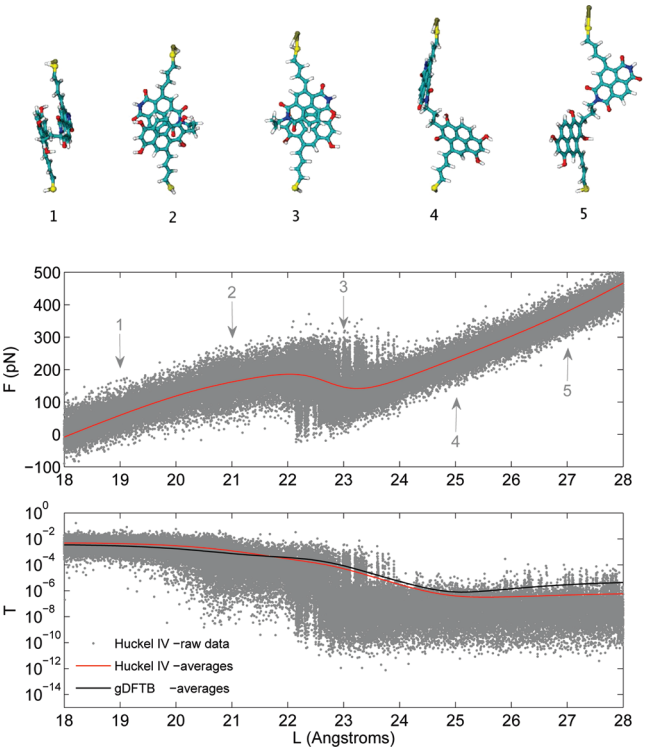

Figure 2. Force exerted F and transmission T during the pulling. Typical structures encountered as L is varied (labels 1−5) are shown in the upper panel. The dots are independent observations, and their distribution arises from thermal fluctuations. The thin solid lines show the average behavior. Note the 3−4 orders of magnitude drop in the conductance of the junction upon unstacking.

leading to fluctuations in the transmission over several orders of magnitude. In the low-transmission regime, the average transmission is dominated by those few members of the ensemble that exhibit higher transmission, a result consistent with previous work on alkanethiols.[18] Such extreme sensitivity to molecular conformation makes the conductance measurements a remarkable probe for the state of the molecule during elongation; this complements information obtained through the force measurements.

Conformational Signatures in the Transport Properties. Additional information about the relationship between molecular conformation and conductance can be gleaned from Figure 3, in which the transmission is shown as a function of the molecular length ξ. A particularly salient feature of the transmission appears near a molecular length of 22 Å, where the average transmission drops by approximately 3 orders of magnitude. This drop corresponds to the complete unfolding of the molecule. The reduction in transmission occurs due to an increase in molecular length and because the primary transport mechanism changes as the molecule goes from a folded to an unfolded configuration.

Such change in transport mechanism can be specified further by examining the contribution of different possible transport modes to the total transmission. Figure 4 shows a decomposition of the gDFTB transmission into local contributions coming from transport between π-stacked moieties (red points) and between various types of hydrogen bonds that may occur as the pulling proceeds (green, purple, and blue points). The insets to each plot highlight the specific interactions that characterize each mode of transport. The transport between the π-stacks is characterized by the sum of local transmission elements between all pairs of atoms

dx.doi.org/10.1021/ja1095396 |J. Am. Chem. Soc. 2011, 133, 2242–2249

colored red, with one member of the pair in one conjugated unit and the partner in the other. In the case of each of the three hydrogen-bonded motifs, the transport is characterized by the specific sums of local transmission elements between the pairs of atoms highlighted in each figure. A conformation is assigned to a particular mode of transport if the absolute value of the sum of selected local transmission elements associated with that conformation is at least 80% of the total transmission. It should be noted that the sums of the local transmission elements in Figure 4 are constructed without reference to any defined surface, but simply by choosing chemically relevant units as defined above. As such, these sums give a qualitative indication of where there are large transmission elements without having a clearly defined relationship with the total transmission. Consequently, a single structure may exhibit multiple modes of transport by this definition. Alternatively, it is possible to plot all the local transmission elements for the molecule averaged over a large number of geometries at fixed molecular length (see Figure S1 in the Supporting Information).

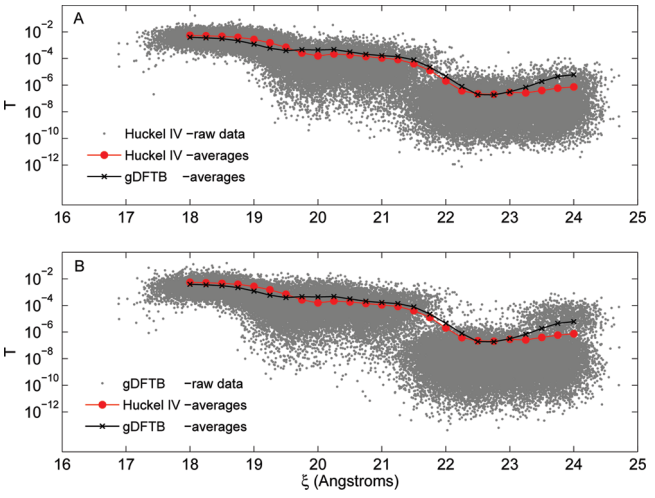

Figure 3. Transmission T as a function of the molecular end-to-end distance ξ. The panels show results obtained using (A) Huckel-IV and (B) gDFTB. The solid lines indicate the average behavior.

As shown in Figure 4, at very short lengths current primarily flows between the stacked aromatic rings (red points). As the molecule is elongated, a new hydrogen bond forms near $\xi = 21$ Å, and coupling between the hydrogen-bonded hydroxy and carbonyl moieties begins to contribute non-negligibly to the average transmission (purple points). When the molecule unstacks, the increasing distance between complementary aromatic rings lessens the relative contribution of $\pi-\pi$ coupling to the overall average transmission, and the breaking of hydrogen bonds reduces the importance of the hydroxy−carbonyl coupling elements. In conformations with $\xi \geq 23$ Å, hydrogen bonding becomes relevant to transport again. A new hydrogen bond forms between the unstacked aromatic entities (blue points), and in the gDFTB results, the average transmission increases by approximately an order of magnitude as a result of the hydrogen-bonded conformations. These results indicate that the effect of hydrogen bonding on transport in the superstacker molecule is two-fold: hydrogen bonds are instrumental in stabilizing the molecule in its folded state, facilitating transport between π-stacks, and the coupling between hydrogen-bonded atoms also may contribute significantly to the average transmission.[41]

There are conformations where through-bond σ transport through the saturated linker dominates; however, these constitute a relatively small fraction of the large-extension conformations and universally exhibit very low levels of transmission. The remainder of the conformations at large extension are characterized by mixed modes of transport and are not readily classified by the qualitative method employed here.

Agreement between Transport Methods. The good agreement between the average transmission values computed using two different computational methods suggests that the findings are robust (see Figure 3). While considerable differences in transmission values may exist for individual conformations, on average the two methods agree quite well. This agreement is particularly surprising if one takes into account that the two

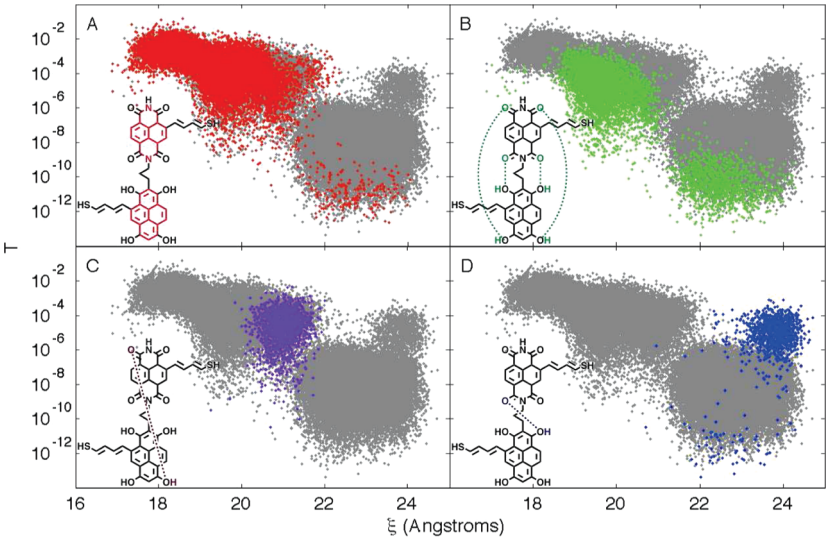

Figure 4. Conformational signatures in the transport properties. The figure highlights geometries where the absolute value of the local contribution to the transmission coming from a particular transport mode is at least 80% of the total gDFTB transmission. The insets specify the different modes of transport considered.

dx.doi.org/10.1021/ja1095396 |J. Am. Chem. Soc. 2011, 133, 2242–2249

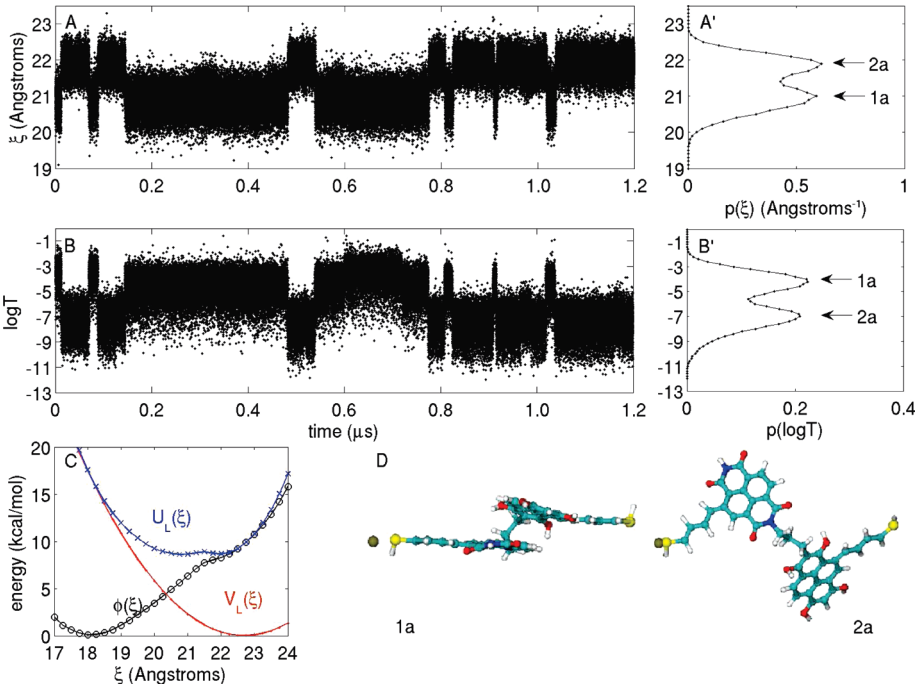

Figure 5. Blinking of the transmission due to bistability in the effective molecule plus cantilever potential. The figure shows the time dependence of (A) the end-to-end molecular extension ξ and (B) the transmission T (Huckel-IV) when L is fixed at 22.7 Å. The associated probability density distributions are shown in (A′) and (B′). At this extension the system blinks between an "on" high-conductance state and an "off" low-conductance state. The bistability arises because the effective potential due to the molecule plus cantilever, $U_L(\xi) = \phi(\xi) + V_L(\xi)$, shown in (C), has a double minimum. Here $\phi(\xi)$ is the molecular potential of mean force along the extension coordinate, and $V_L(\xi) = (k/2)(\xi - L)^2$ is the cantilever potential. Representative structures of the two modes of the dynamics are shown in (D).

methods employed use a different description of the electronic structure, different basis sets, and different treatments of the metal electrodes that can lead to stark disparities.[42] A notable exception to this agreement occurs for long molecular lengths where hydrogen bonding is the sole transport mode determining average transmission. The disagreement stems from the different treatment of hydrogen bonding in the two methods (see Figure S2 in the Supporting Information). Further comparison of the transmission spectra computed from the two methods can be found in Figure S3 of the Supporting Information.

Blinking in the Transmission. For extensions L around the unfolding region, the dynamics of the junction exhibits a bistability in which the molecule repeatedly stacks and unstacks. This dynamical behavior is illustrated in Figure 5, which shows the time dependence of the molecular end-to-end distance (panel A) and the resulting Huckel-IV transmission (panel B) when L = 22.7 Å. The right panels in Figure 5 show the probability density distribution of the ξ and log T measurements. As shown, the system exhibits a clear dynamical bistability along the ξ coordinate. This bistability leads to sharp blinking in the conductance measurements from a high-transmission to a low-transmission state. The high-transmission state coincides with circumstances where the molecule is stacked.

The origin of this dynamical bistability can be understood as follows. The partition function of the molecule plus cantilever at a given extension L can be expressed as[22]

$$Z(L) = \alpha \int d\xi \exp\{-\beta[\phi(\xi) + V_L(\xi)]\} \qquad (5)$$

where $\phi(\xi)$ is the molecular potential of mean force—the Helmholtz free energy profile—along the end-to-end distance coordinate, $V_L(\xi) = k(\xi - L)^2/2$ is the potential due to the cantilever of stiffness k at extension L, $\beta = 1/k_B T$ is the inverse temperature, and α is a constant factor that is irrelevant for the present purposes. Equation 5 implies that the extension process can be viewed as thermal motion along a one-dimensional effective potential given by $U_L(\xi) = \phi(\xi) + V_L(\xi)$. Any bistability observed during the dynamics must manifest as a double minimum in $U_L(\xi)$.

Figure 5C shows $\phi(\xi)$, $V_L(\xi)$, and $U_L(\xi)$ when L is fixed at 22.7 Å. The molecular potential of mean force consists of two convex regions that represent the molecular folded and unfolded conformations and a region of concavity around ξ = 21.5 Å where the molecule unfolds. In the presence of the bias due to the cantilever (red line) this region of concavity turns into a barrier, leading to bistability in $U_L(\xi)$ (in blue) and causing the observed blinking in the conductance and force measurements. By changing L, the relative thermal weights of the folded and unfolded conformations can be manipulated, leading to control over the conductance properties of the junction.

Role of the Cantilever Stiffness. Since the mechanical properties measured during the pulling are for the molecule plus cantilever, the observed extension behavior depends on the stiffness of the cantilever employed.[22] How does this affect the basic features of the molecular switch? Figure 6 shows the probability density distribution $p_L(\log T)$ in the log T measurements when the pulling is performed using cantilevers of different stiffness. As shown, both the drop in the conductance upon molecular unfolding and the bistability for selected extensions remain robust to changes of at least 3 orders of magnitude in the cantilever stiffness. Naturally, by reducing k, a larger L is required to go from the high-transmission to the low-transmission state,

dx.doi.org/10.1021/ja1095396 |J. Am. Chem. Soc. 2011, 133, 2242–2249

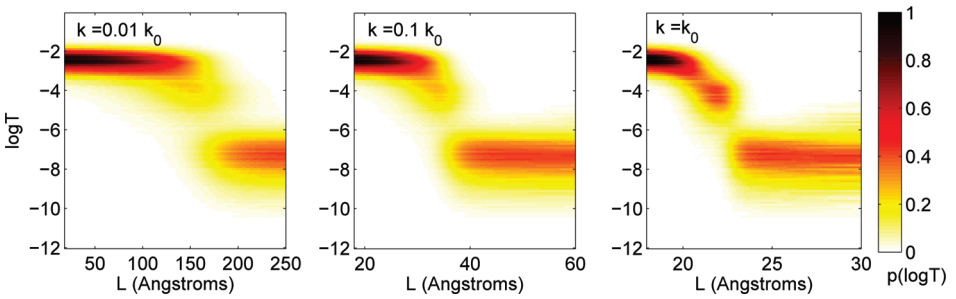

Figure 6. Robustness of the conductance switching to changes in the cantilever stiffness. The figure shows the probability density distributions of the transmission $p_L(\log T)$ when cantilevers of different stiffness are employed in the pulling. The cantilever force constants are expressed in terms of $k_0 = 1.1$ N/m, the stiffness employed in the pulling simulations. The quantity $p_L(\log T)$ was estimated using the data shown in Figure 2. Note the difference in scales along the x-axis.

but the two phases of the conductance switch remain distinct. We note, however, that the blinking is expected to decay when very stiff cantilevers are employed since under such conditions a double minimum in the effective potential $U_L(\xi)$ cannot develop.[22]

FINAL REMARKS

In this contribution we have computationally demonstrated how the integration of molecular electronics with single-molecule pulling techniques can lead to the design of mechanically activated molecular switches in which an AFM is used to induce changes in the molecular conductance by generating changes in the molecular conformation. In the specific example considered, the switching mechanism relies on unfolding a molecular superstacker—a π-stacker with a folded conformation further stabilized by four hydrogen bonds—an event that results in a 3−4 orders of magnitude drop in the average conductance that is concurrent with a drop in the average force. The resulting switch is reversible and robust to changes in the cantilever stiffness. Further, both the "on" and "off" phases are within the observable conductance range.[14]

In the broadest sense, any nanostructure that shows a strong dependence of the transmission on geometry could be described as a switch. For example, a flexible alkane molecule can display distance-dependent conductance when pulled,[18,43,44] or a STM break junction can switch between a large transmission state in contact and a weak transmission state when broken. The prototype presented here differs from these examples in the sense that the switching transition due to molecular bistability is both sharp and reversible. This contrasts with alkane elongation, in which the transition is reversible but not sharp, and STM break junctions, in which the transition is sharp but not reversible.

The precise geometry of the tip and the surface, surface deformation, and possible shifts in the thiol binding sites during extension may all influence the details of any transport measurement and have not been considered explicitly in this work. Prior theoretical studies have illustrated the extension and deformation that may occur as a molecule with a terminal thiol bound to gold clusters is pulled away from a gold tip.[45,46] Measurements[16] and simulations[44] suggest that conductance modulation as a result of binding site variation is modest with respect to the dramatic drop in the conductance due to unstacking. Similarly, possible restructuring of the gold electrodes[47] and/or thiol−gold bond breaking[48] during pulling typically require forces of 1.0−1.5 nN that are substantially larger than the average force needed to unfold the stacker (0.186 nN) and, thus, are not expected to be dominant effects either. This hierarchy of forces is typical of single-molecule pulling experiments.

Since the potential of mean force of the π-stacker has a region of concavity along the extension coordinate ξ (a feature that is typical of molecules with stable folded conformations), it is possible to find cantilever extensions L where the potential of the molecule plus cantilever is bistable along ξ. At such extensions the molecule constantly folds and unfolds, leading to blinking between a high-transmission/high-force and a low-transmission/low-force regime. The time scale for the blinking can be slowed by cooling or tuned by further chemical manipulation. We identify such blinking as a characteristic signature of mechano-electric nanojunctions.

The simulations reflect the remarkable sensitivity of the conductance to changes in the molecular conformation. Such sensitivity can be used to characterize the state of the molecule as it is mechanically elongated, complementing any information obtained through force measurements. Interestingly, the thermal distribution of conductance measurements during the extension computed by two largely different transport methods exhibit excellent agreement, even when the two methods disagree for individual conformations within the thermal ensemble.

Both of these methods neglect vibronic coupling in the description of the transport, and further the molecular geometry is assumed to be static on the time scale of the electron transfer event. In systems where destructive quantum interference is responsible for the low conductance, these effects may be anticipated to have a significant impact by opening inelastic transport channels[49] and dephasing effects.[50] It should be noted that destructive interference in the electron transport is not relied upon in this case, but nevertheless the inclusion of inelastic transport and dephasing effects may change the magnitude of the transport through both the folded and unfolded configurations.

Specific conformational signatures in the conductance vs extension map of the π-stacker were discerned using a local current analysis.[38,42] The analysis unveiled contributions from π-stacking and from the making and breaking of hydrogen bonds to the conductance (in a rather complex data set). Local current analysis can also provide significant insight into mechanisms for chemical control of conduction characteristics. For instance, the local partitioning of the gDFTB results suggests that, by removing the single H-bond responsible for high transmission at long extensions, one may increase the

dx.doi.org/10.1021/ja1095396 |J. Am. Chem. Soc. 2011, 133, 2242–2249

"on/off" ratio of the switch without significantly disrupting the stability of the stacker.

Careful device design requires an appreciation of the role that components play in both the structural stability and the transport properties. The methods employed herein provide a clear demonstration of these effects. The dual role of hydrogen bonds in stabilizing the folded conformation, thereby facilitating high levels of π transport, and also directly participating as active pathways for current flow is particularly intriguing. Understanding the importance of these types of interactions provides an opportunity to unravel the structure−function relationships that govern molecular folding and conductance in a dynamic and flexible system.

The basic behavior illustrated by the simulations is expected to be common to a large variety of mechanically activated molecular devices. The results and insights presented might lead to the development of a series of novel mechanically controlled molecular devices. Future prospects include the use of external stimuli as an active switching component, pulling systems where incoherent transport is dominant, and identifying cases where the conductance actually increases with extension.

■ ASSOCIATED CONTENT

Supporting Information. Additional force field parameters, the transmission through hydrogen bonds as described by gDFTB and Huckel-IV, a comparison of the gDFTB and Huckel-IV transmission spectra for selected conformations, and the average local transmission elements for the molecule at several molecular lengths. This material is available free of charge via the Internet at http://pubs.acs.org.

■ AUTHOR INFORMATION

Corresponding Author
ifranco@chem.northwestern.edu; ratner@chem.northwestern.edu

■ ACKNOWLEDGMENT

This work was supported by the Non-equilibrium Energy Research Center (NERC), which is an Energy Frontier Research Center funded by the U.S. Department of Energy, Office of Science, Office of Basic Energy Sciences under Award Number DE-SC0000989. The work was partly supported by the Chemistry Division of the NSF. C.B.G.. is supported by a Graduate Research Fellowship from the NSF. G.C.Solomon gratefully acknowledges funding from The Danish Council for Independent Research|Natural Sciences.

■ REFERENCES

(1) Ritort, F. *J. Phys.: Condens. Matter* **2006**, *18*, R531–R583.
(2) Rief, M.; Gautel, M.; Oesterhelt, F.; Fernandez, J. M.; Gaub, H. E. *Science* **1997**, *276*, 1109–1112.
(3) Liphardt, J.; Onoa, B.; Smith, S. B.; Tinoco, I.; Bustamante, C. *Science* **2001**, *292*, 733–737.
(4) Oberhauser, A. F.; Hansma, P. K.; Carrion-Vazquez, M.; Fernandez, J. M. *Proc. Natl. Acad. Sci. U.S.A.* **2001**, *98*, 468–472.
(5) Evans, E. *Annu. Rev. Biophys. Biomol. Struct.* **2001**, *30*, 105–128.
(6) Bustamante, C.; Liphardt, J.; Ritort, F. *Phys. Today* **2005**, *7*, 43–48.
(7) Datta, S. *Quantum transport: Atom to transistor*; Cambridge University Press: New York, 2005.
(8) Joachim, C.; Gimzewski, J. K.; Aviram, A. *Nature* **2000**, *408*, 541–548.
(9) Nitzan, A. *Annu. Rev. Phys. Chem.* **2001**, *52*, 681–750.
(10) Nitzan, A.; Ratner, M. A. *Science* **2003**, *300*, 1384–1389.
(11) Joachim, C.; Ratner, M. A. *Proc. Natl. Acad. Sci. U.S.A.* **2005**, *102*, 8801–8808.
(12) Galperin, M.; Ratner, M. A.; Nitzan, A.; Troisi, A. *Science* **2008**, *319*, 1056–1060.
(13) Chen, F.; Tao, N. J. *Acc. Chem. Res.* **2009**, *42*, 429–438.
(14) Lafferentz, L.; Ample, F.; Yu, H.; Hecht, S.; Joachim, C.; Grill, L. *Science* **2009**, *323*, 1193–1197.
(15) Chang, S.; He, J.; Kibel, A.; Lee, M.; Sankey, O.; Zhang, P.; Lindsay, S. *Nature Nanotechnol.* **2009**, *4*, 297–301.
(16) Quek, S. Y.; Kamenetska, M.; Steigerwald, M. L.; Choi, H. J.; Louie, S. G.; Hybertsen, M. S.; Neaton, J. B.; Venkataraman, L. *Nature Nanotechnol.* **2009**, *4*, 230–234.
(17) Parks, J. J.; Champagne, A. R.; Costi, T. A.; Shum, W. W.; Pasupathy, A. N.; Neuscamman, E.; Flores-Torres, S.; Cornaglia, P. S.; Aligia, A. A.; Balseiro, C. A.; Chan, G. K.-L.; Abruña, H. D.; Ralph, D. C. *Science* **2010**, *328*, 1370–1373.
(18) Lin, J.; Beratan, D. N. *J. Phys. Chem. A* **2004**, *108*, 5655–5661.
(19) Gunari, N.; Balazs, A. C.; Walker, G. C. *J. Am. Chem. Soc.* **2007**, *129*, 10046–10047.
(20) Imparato, A.; Sbrana, F.; Vassalli, M. *Europhys. Lett.* **2008**, *82*, 58006.
(21) Kirmizialtin, S.; Huang, L.; Makarov, D. E. *J. Chem. Phys.* **2005**, *122*, 234915.
(22) Franco, I.; Schatz, G. C.; Ratner, M. A. *J. Chem. Phys.* **2009**, *131*, 124902.
(23) Elstner, M.; Porezag, D.; Jugnickel, G.; Elsner, J.; Haugk, M.; Frauenheim, T.; Suhai, S.; Seifert, G. *Phys. Rev. B* **1998**, *58*, 7260–7268.
(24) Frauenheim, T.; Seifert, G.; Elstner, M.; Hagnal, Z.; Jungnickel, G.; Porezag, D.; Suhai, S.; Scholz, R. *Phys. Status Solidi B* **2000**, *217*, 41–62.
(25) Frauenheim, T.; Seifert, G.; Elstner, M.; Niehaus, T.; Koehler, C.; Amkreutz, M.; Sternberg, M.; Hajnal, Z.; Di Carlo, A.; Suhai, S. *J. Phys.: Condens. Matter* **2002**, *14*, 3015–3047.
(26) Porezag, D.; Frauenheim, T.; Kohler, T.; Seifert, G.; Kaschner, R. *Phys. Rev. B* **1995**, *51*, 12947–12957.
(27) Pecchia, A.; Di Carlo, A. *Rep. Prog. Phys.* **2004**, *67*, 1497–1561.
(28) Zahid, F.; Paulsson, M.; Datta, S. . *Advanced Semiconductors and Organic Nanotechniques*; Academic Press: New York, 2003; Vol. 3, Chapter 1, pp 1−41.
(29) Ponder, J. *TINKER: Software tools for molecular design 4.2*; Washington University School of Medicine: Saint Louis, MO, 2004.
(30) Allinger, N. L.; Yuh, Y. H.; Lii, J. H. *J. Am. Chem. Soc.* **1989**, *111*, 8551–8566.
(31) Lii, J. H.; Allinger, N. L. *J. Am. Chem. Soc.* **1989**, *111*, 8566–8575.
(32) Lii, J. H.; Allinger, N. L. *J. Am. Chem. Soc.* **1989**, *111*, 8576–8582.
(33) Bilic, A.; Reimers, J. R.; Hush, N. S. *J. Chem. Phys.* **2005**, *122*, 094708–094715.
(34) Xue, Y.; Datta, S.; Ratner, M. A. *J. Chem. Phys.* **2001**, *115*, 4292–4299.
(35) Ghosh, A. W.; Zahid, F.; Datta, S.; Birge, R. R. *Chem. Phys.* **2002**, *281*, 225–230.
(36) Zahid, F.; Paulsson, M.; Polizzi, E.; Ghosh, A. W.; Siddiqui, L.; Datta, S. *J. Chem. Phys.* **2005**, *123*, 064707.
(37) Todorov, T. N. *J. Phys.: Condens. Matter* **2002**, *14*, 3049–3084.
(38) Solomon, G. C.; Herrmann, C.; Hansen, T.; Mujica, V.; Ratner, M. A. *Nature Chem.* **2010**, *2*, 223–228.
(39) Ferrenberg, A. M.; Swendsen, R. H. *Phys. Rev. Lett.* **1989**, *63*, 1195–1198.
(40) Kumar, S.; Bouzida, D.; Swendsen, R. H.; Kollman, P. A.; Rosenberg, J. M. *J. Comput. Chem.* **1992**, *13*, 1011–1021.
(41) Beratan, D. N.; Onuchic, J. N.; Hopfield, J. J. *J. Chem. Phys.* **1987**, *86*, 4488–4498.
(42) Andrews, D. Q.; Solomon, G. C.; Van Duyne, R. P.; Ratner, M. A. *J. Am. Chem. Soc.* **2008**, *130*, 17309–17319.

(43) Li, C.; Pobelov, I.; Wandlowski, T.; Bagrets, A.; Arnold, A.; Evers, F. *J. Am. Chem. Soc.* **2008**, *130*, 318–326.
(44) Paulsson, M.; Krag, C.; Frederiksen, T.; Brandbyge, M. *Nano Lett.* **2009**, *9*, 117–121.
(45) Krüger, D.; Rousseau, R.; Fuchs, H.; Marx, D. *Angew. Chem., Int. Ed.* **2003**, *42*, 2251–2253.
(46) Konôpka, M.; Rousseau, R.; Štich, I.; Marx, D. *J. Am. Chem. Soc.* **2004**, *126*, 12103–12111.
(47) Rubio-Bollinger, G.; Bahn, S. R.; Agraït, N.; Jacobsen, K. W.; Vieira, S. *Phys. Rev. Lett.* **2001**, *87*, 026101.
(48) Grandbois, M.; Beyer, M.; Rief, M.; Clausen-Schaumann, H.; Gaub, H. E. *Science* **1999**, *283*, 1727–1730.
(49) Skourtis, S. S.; Waldeck, D. H.; Beratan, D. N. *J. Phys. Chem. B* **2004**, *108*, 15511–15518.
(50) Nitzan, A. *Annu. Rev. Phys. Chem.* **2001**, *52*, 681.